Civil Engineering Faculty Publications   Civil Engineering

2016

Expedient airfield runway repair using folded fiberglass mat

Christopher Y. Tuan
University of Nebraska-Lincoln, ctuan1@unl.edu

Willaim C. Dass
Applied Research Associates, Albuquerque, NM

Expedient airfield runway repair using folded fiberglass mat

Christopher Y. Tuan[1] and William C. Dass[2]

1 Civil Engineering Department, University of Nebraska–Lincoln, 203F Peter Kiewit Institute, 1110 South 67th Street,
    Omaha, NE 68182- 0178, USA
2 Applied Research Associates (ARA), 4300 San Mateo Blvd. NE Suite A-220, Albuquerque, NM 87110, USA

Corresponding author — C. Y. Tuan, email ctuan1@unl.edu

Abstract

For expedient airfield runway repair, the US Air Force has developed a folded fiberglass mat to cover craters repaired with a well-compacted granular base material. The objective of this study was to evaluate the adequacy of using polymer plugs to anchor the mat to a repaired asphalt pavement for heavy aircraft operations. The effort consisted of materials testing, field experiments and analytical modeling. An 89,800-kg (198,000-pound) load cart having the footprint of a single C-5 main gear was pulled on a mat with wheels locked to simulate full braking forces. Anchor bushings were instrumented to measure anchor loads. A simplified numerical model was developed for anchor load analysis which has been validated against the load cart test data. The anchor system sustained the braking forces from all the load cart tests without failure. The polymer plug anchors have adequate vertical pull-out capacity to resist the uplifting force from the "bow wave" formation of the mat. The polymer plug anchors also have adequate resistance to fatigue loads.

Keywords: airfield runway repair, fiberglass mat, anchors, braking force, modeling, field experiments, instrumentation

Introduction

General operations for airfield damage repair by the various US military services are given in UFC 3-270-07 (Unified Facilities Criteria 2003). For expedient airfield runway repair, the US Air Force has developed a folded fiberglass mat (FFM) to cover craters repaired with a well-compacted granular base material for fighter aircraft operations. As shown in Figure 1, an FFM consists of nine panels and each panel is 1.8m (6 ft) wide, 9m (30 ft) long and about 5mm (0.2 in) thick. Adjacent panels are connected by 76mm (3 in) wide flexible fiber-reinforced elastomer hinges. When folded, the mat assembly is 1.8m (6 ft) wide, 9m (30 ft) long, about 254mm (10 in) thick and weighs about 1360 kg (3000 lbs). Each panel is secured in the pavement by three anchors at 61 cm (2 ft) spacing along all four edges of the mat. The specifications of the FFM fabrication and packaging are given in MILDTL- 32265 (2007), and those for inspection and repair of FFM damage are given in the Engineering Technical Letter (ETL 07-10 2007). Schemes for anchoring the FFM will depend on the type of runway pavement: 1.3-cm (0.5- in) diameter, 14-cm (5.5-in) long rock bolts with a 1.9-cm (0.75-in) diameter sleeve are used for concrete pavements; 1.6-cm (0.625 in) diameter, 24-cm (9.5 in) long rock bolts with a 1.9-cm (0.75-in) diameter sleeve for asphalt-overlaid concrete pavements; and 24-cm (9.5-in) long rock bolts in a 3.8-cm (1.5-in) diameter polymer plug for asphalt pavements. The polymer used is a two-part polyurethane

mix that reacts rapidly to form a solid with 20.7 MPa (3000 psi) compressive strength in less than 5 min at 22°C (72°F). Specific requirements on the anchors and polymer plugs are given in the Engineering Technical Letter (ETL 07-2 2007).

Air Force operations may require that a mix of aircraft types (fighters, tankers, cargo and bombers) operate from an airbase. The FFM is currently certified by the Air Force for use to cover repaired craters for all fighter jet aircraft and cargo aircraft up to the C-130. Therefore, the FFM and its anchors must also have adequate capacity for heavy cargo aircraft operations over thin asphalt pavements, potentially <13 cm (5 in). If the existing anchors are adequate for all Air Force aircraft, there would be more logistic options for using the FFM.

The objective of this research was to evaluate the mat-anchoring capacity of the polymer plugs in asphalt concrete pavements, under simulated braking forces from a cargo aircraft. The scope of work consisted of materials testing, field experiments and analytical modelling.

Analytical studies

When an aircraft is taxiing at high speed (e.g. 168 km/h, 90 knots, 104 mph) after landing, the weight supported by its main gear is reduced by the airlift (Lester and Phil 1973). This reduced weight is called the "effective weight." Modern US Air Force cargo aircrafts, such as the C-5 and the C-17, are equipped with anti-skid brakes that allow wheels
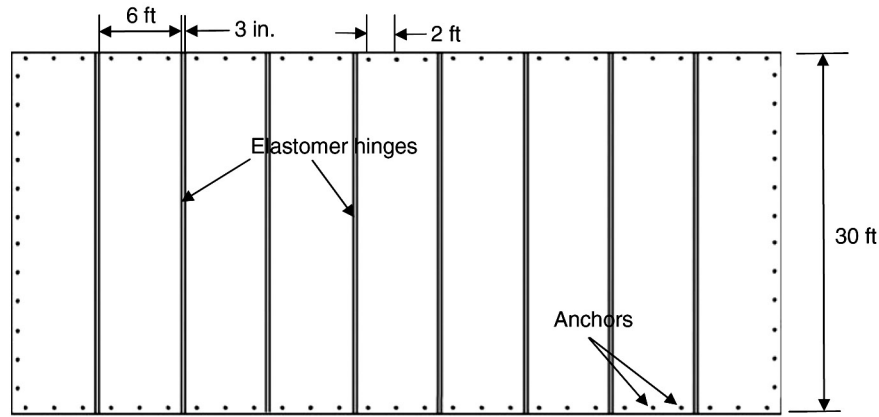
1 ft = 30.48 cm; 1 in. = 2.54 cm.

Figure 1. Typical layout of an FFM.

to rotate when a preset frictional force limit is exceeded. Therefore, using the statically applied braking forces under the maximum aircraft weight would simulate a "skidding" or worst-case scenario with the full extent of horizontal braking forces.

A complex mechanical system is often analyzed by using a lumped parameter model (Marzbanrad and Pahlavani 2011). The horizontal braking forces exerted on a mat by a moving aircraft depend upon the effective weight on the main gear and the coefficient of friction between the tires and the mat. These horizontal forces are resisted by the friction between the mat and the repaired pavement surface, and by the tensile, compressive and shear forces developed in the mat. These in-plane mat forces are, in turn, carried by the anchors in the pavement. Based on this load-transfer mechanism, a simplified model was developed for anchor load predictions. A more comprehensive finite element model of the aircraft tire–mat–anchor–pavement system was also developed to investigate the buckling behavior of the mat in front of the tires.
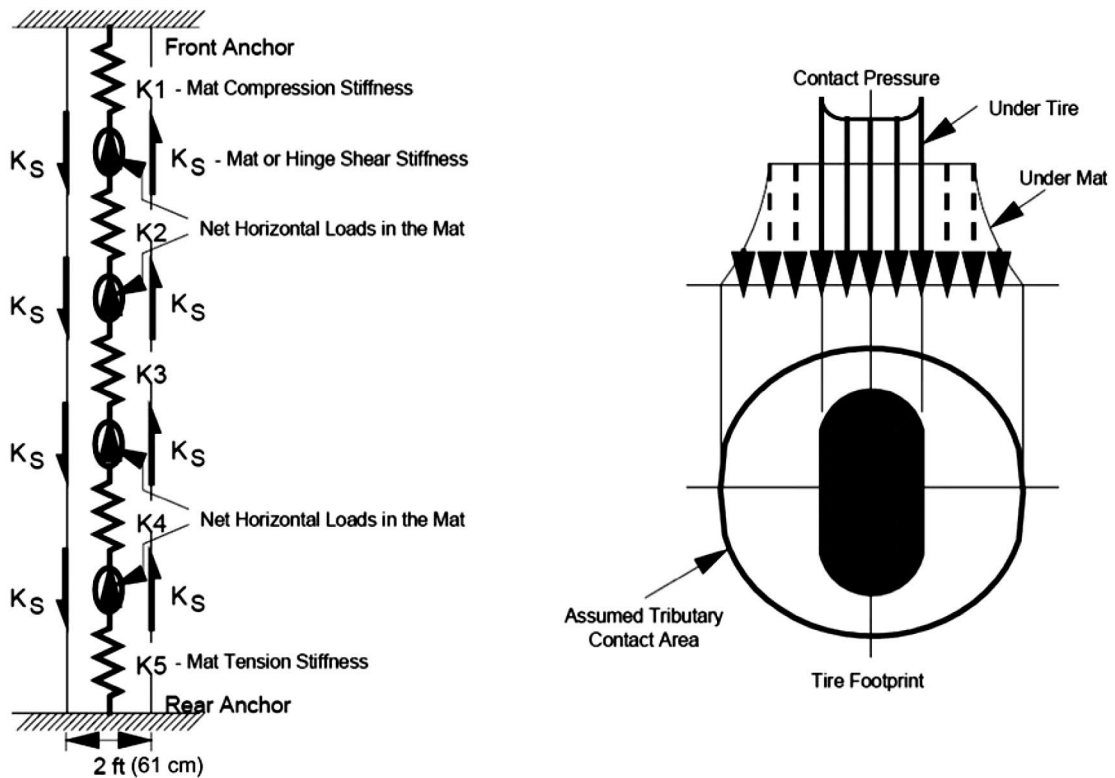

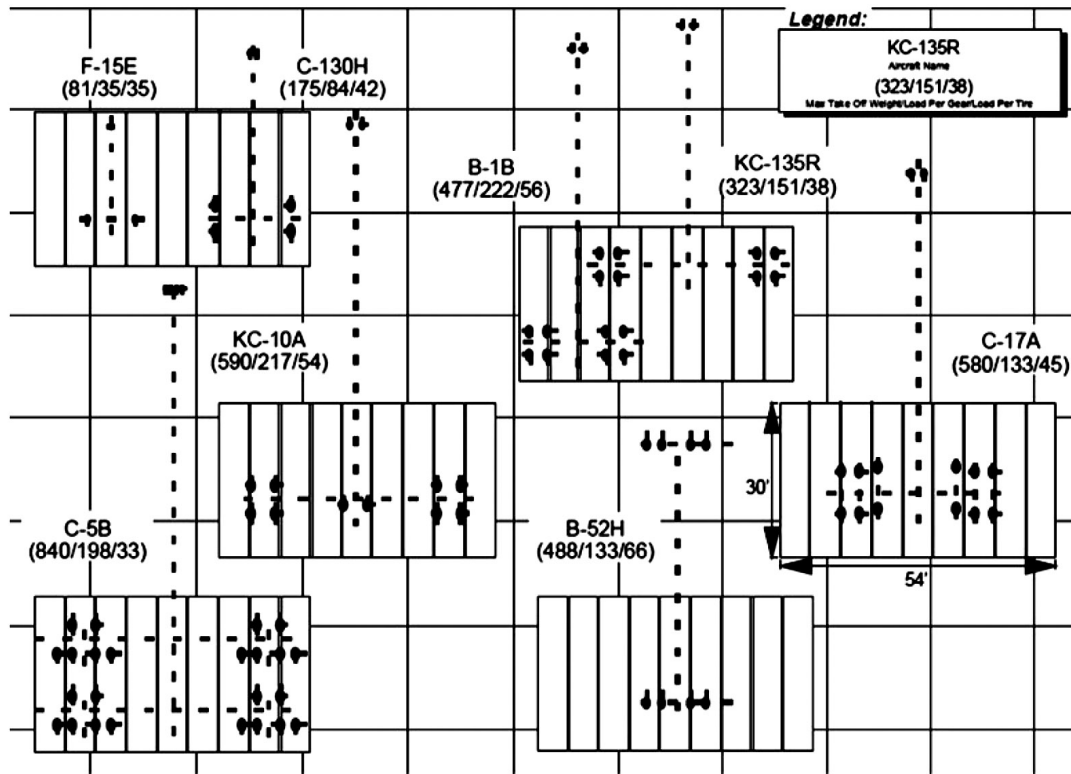**Figure 2.** A lumped-parameter model for anchor load analysis.

Figure 3. US Air Force aircraft gear configurations.

A simplified model for anchor load analysis

The model, using a lumped-parameter approach (i.e. a spring–mass system), is illustrated in Figure 2. The fiberglass mat is divided into 27 61-cm (2-ft) wide, 9-m (30-ft) long strips, with four potential tire contact (or wheel load) locations on each strip. A linear spring at each end of the strip is used to model the anchor stiffness. Horizontal braking forces are applied at the appropriate wheel locations. These horizontal forces represent the net frictional forces applied on the mat, which is the tire/mat friction minus the mat/pavement friction. The horizontal forces are resisted by the shear forces in the fiberglass mat panels and elastomer hinges, the compressive forces in front of the tires and the tensile forces behind the tires in the plane of the mat. The mat-compressive stiffness is greatly reduced when the mat buckles in front of the tires. A system of 54 simultaneous algebraic equations, based on force equilibrium, was established to solve for the unknown front and rear anchor loads. This simple model has the flexibility to accommodate the footprint of any aircraft of interest and has proven to be very useful for quickly evaluating the effects of varying aircraft type, location and other important parameters.

Model parameters

Essential parameters that affect anchor loads include (1) aircraft gear configuration, (2) aircraft weight, (3) aircraft

position on the mat, (4) mat configuration (i.e. single mat vs. multiple mats), (5) coefficient of friction between tires and mat, (6) coefficient of friction between mat and repaired crater, (7) crater geometry, (8) crater position with respect to the mat, (9) material properties of the fiberglass mat, (10) material properties of the underlying repaired crater, (11) material properties of the pavement and (12) stiffness and strength characteristics of the anchor bolt in the pavement.

Each aircraft has unique characteristics such as gear loads, gear configuration, and tire pressure and contact area. By analyzing the critical aircraft for each Air Force aircraft classification group and overlaying their load and gear configurations on an FFM as shown in Figure 3, the C-5 was found to produce the most severe horizontal anchor loads upon braking. Eight of the 12 tires of the main gear could be on a panel at the same time. Holliway and Millard (1990) provided detailed Air Force aircraft weights and dimensions.

Laboratory and field tests have been conducted to provide realistic parameters for the analytical studies. The numerical values of these parameters are given herein.

Mechanical properties of the fiberglass mat

Four standard, uniaxial tensile tests were conducted to determine the elastic tensile modulus of the fiberglass mat. The coupons were cut out from fiberglass mat panels such that their lengths were parallel to the hinges, which are the directions of aircraft traffic. The average tensile modulus
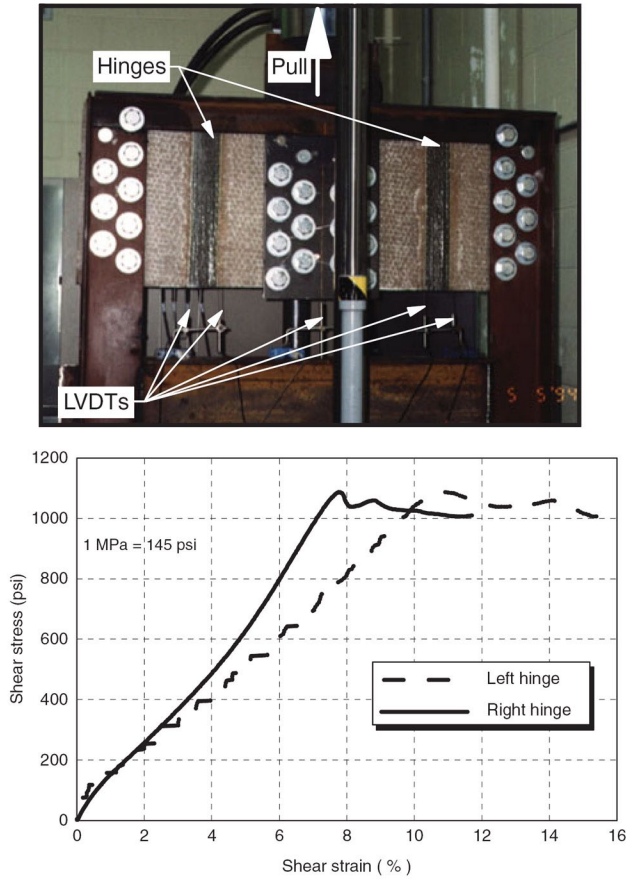
Figure 4. Direct shear test on elastomer hinges.

Figure 5. A 7.6-m diameter, 457-mm deep artificial crater in asphalt test pad.

calculated from the resulting stress–strain curves was about 7 GPa (1,000,000 psi), which compares reasonably well with the 10 GPa (1,450,000 psi) value previously reported by Law Engineering (1988). A Poisson's ratio of 0.426 was also reported by Law Engineering (1988) for the fiberglass mat. Even though the fiberglass mat may exhibit orthotropic material response, it is sufficiently accurate to assume linearly elastic behavior in the direction parallel to the hinges. In addition, a special test was conducted to determine the stiffness and the strength parameters of the elastomer hinges under shear. The set-up of this hinge shear test is illustrated in Figure 4. The hinges are approximately 8 cm (3 in) wide. Linear variable displacement transducers (LVDTs) were used to determine the relative displacements between the two edges of each hinge while the center fiberglass mat piece was pulled upward. The shear stiffness of the hinge was calculated directly from the linear portion of the load–displacement data to be about 1146 kN/m (6540 lbs/in). Average shear stress was determined by dividing half the applied load by the nominal hinge cross-sectional area, while the average shearing strain was determined by dividing the relative displacements by the width of the hinge. This shear stress– strain relation of the hinge material is presented in Figure 4.
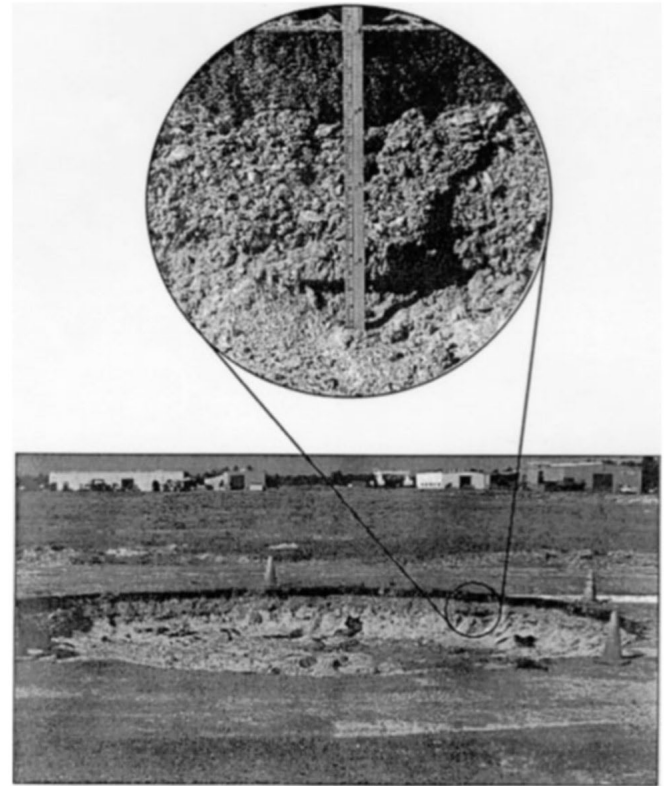
Interface friction coefficients

The friction coefficients at the tire/mat/pavement interfaces are also essential modelling parameters. These coefficients were measured in full-scale field tests.

Between fiberglass mat and asphalt pavement. An asphalt pavement test site located at Tyndall Air Force Base, Florida, USA, was selected for field tests. As shown in Figure 5, excavation of the test site revealed that the pavement consisted of a 107-mm (4.2-in) dense-graded asphalt surface layer over an oyster shell base course approximately 267mm (10.5 in) thick. The subgrade was free-draining beach sand with a fluctuating water table.

Static pull tests were conducted to determine the mat-to-asphalt pavement interface coefficient of friction, using an 89,800-kg (198,000-lb) C-5 load cart placed on the center of an unanchored fiberglass mat. The test set-up is shown in Figure 6, where the load cart has the footprint of a single C-5 main gear. Each wheel carried 147 kN (33,000 lbs) and the tire inflation pressure was 1 MPa (145 psi). All six wheels of the load cart were locked while a horizontal pulling force was gradually applied to the load cart until the mat slipped abruptly across the pavement. Bulldozers were chained in series with wire ropes and parked in a sand pit to provide
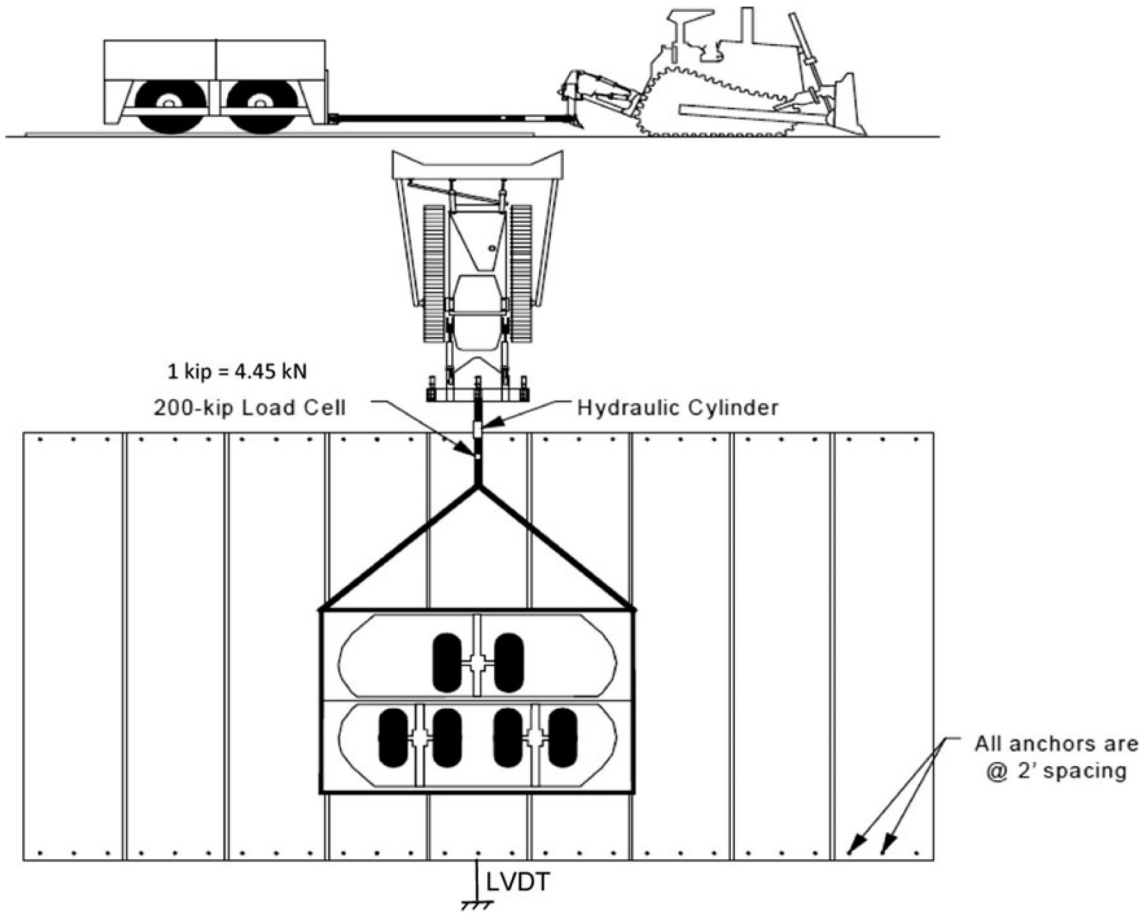
Figure 6. Load cart test set-up.

anchorage for the pulling force. The mat displacement was measured with an LVDT and the pulling force was measured with a load cell. The peak pulling forces along with the corresponding mat displacements measured are summarized in Table 1. As shown in Figure 2, friction forces only exist where there is contact pressure between the mat and the pavement. Thus, the frictional resistance in the interface can be treated as if they were concentrated at the tire locations. An "apparent" coefficient of friction may be calculated by dividing the peak pulling force by the total wheel loads (i.e. 881 kN (198,000 lbs)). The coefficients of friction thus obtained from the five pull tests, with an average value of 0.564, are also given in Table 1.

Between fiberglass mat and repaired crater. The asphalt test site was excavated to create a 7.6-m (25-ft) diameter, 457-mm (18-in) deep artificial crater and repaired according to standard procedures using a well-graded aggregate mix per ASTM D2940. The granular base material was well compacted by a road construction roller until the top of the repair was flush with the asphalt pavement. The 89,800-kg (198,000-lb) C-5 load cart was placed on an unanchored fiberglass mat over the repaired crater. Three static pull tests were conducted to determine the coefficient of friction between the fiberglass mat and the repaired crater. The peak forces measured when the unanchored mat slipped abruptly over the repaired crater are given in Table 2. It was

Table 1. Coefficient of friction between FFM and asphalt pavement.

Test number	Peak force kN (kip)	Mat displacement mm (in)	Coefficient of friction
1	498 (112)	108 (4.25)	0.566
2	521 (117)	124 (4.87)	0.591
3	516 (116)	121 (4.75)	0.586
4	432 (97)	64 (2.50)	0.490
5	516 (116)	108 (4.25)	0.586
Average	498 (112)	105 (4.12)	0.564

Table 2. Coefficient of friction between FFM and repaired crater.

Test number	Peak force kN (kip)	Coefficient of friction
1	530.4 (119.2)	0.602
2	573.6 (128.9)	0.651
3	590.5 (132.7)	0.670
Average	564.7 (126.9)	0.641

Table 3. Coefficient of friction between C-5 tires and fiberglass mat.

Test number	Peak force kN (kip)	Coefficient of friction
1	580.3 (130.4)	0.658
2	581.6 (130.7)	0.660
3	576.3 (129.5)	0.654
4	578.5 (130.0)	0.657
5	583.8 (131.2)	0.662
6	599.9 (134.8)	0.681
Average	583.4 (131.1)	0.662
Small-scale test	5.215 (1.172)	0.670

suspected that the settlement of the repair material caused higher pulling forces in the latter two tests. Removal of the mat after the pull tests revealed that the repaired crater had about 76mm (3 in) deep ruts caused by the heavy wheel loads. The coefficients of the "apparent" friction for these tests are also given in Table 2. It appears that this "apparent" friction would increase due to rutting in the repaired crater under the load cart loads, because a vertical force component would be required to pull the wheels upward and out of the ruts. However, these ruts would not form in real operations where the aircraft wheels would wander over the mat and the wheel loads would last for a much shorter duration than in the load cart tests.

Between C-5 tires and fiberglass mat. The tire-to-mat interface coefficient of friction was estimated from the C-5 load cart test data. A fiberglass mat was placed on the asphalt test site and secured with 54 anchors. With the wheels locked up, a pulling force was gradually applied using a hydraulic cylinder such that the peak value at which load cart skidded on the mat could be readily determined. The peak forces along with the corresponding coefficients of friction are given in Table 3. An additional test was conducted using a 103-cm^2 (16-in^2) flat piece of tire attached to the bottom of a 7788-N (1750-lb) lead weight and pulled across a fiberglass mat surface. The average coefficient of friction of 0.662 from the load cart tests compares very well with the 0.67 value measured in the additional small-scale test. These values are summarized in Table 3.

Material properties of asphalt pavement and oyster shell base

Core samples taken from the test site were analyzed to provide the material properties of the pavement. The asphalt pavement layer was about 102mm (4 in) thick, with a unit weight of 2240 kg/m^3 (140 pcf). Although the mechanical properties of an asphaltic concrete are highly dependent on the ambient temperature, the asphalt pavement at the test site was estimated to have an elastic modulus of 1.03 GPa (150,000 psi) and a Poisson's ratio of 0.35. The oyster shell base course was about 254mm (10 in) thick with a unit

Front View

Side View

Figure 7. Bow wave formation under heavy wheel loads.

weight of 1440 kg/m^3 (90 pcf), and was estimated to have an elastic modulus of 1.03 GPa (15,000 psi) and a Poisson's ratio of 0.45. These moduli and Poisson's ratios were obtained based on the test data obtained using a falling weight deflectometer and back-calculated by trial and error with a layered elastic analysis computer program: Jacob Uzan Layered Elastic Analysis (Barker and Gonzalez 1991).

Uplifting force due to mat bulging

When a heavy aircraft passes over the mat, a depression basin forms under the wheel loads. If the wheels are locked up, the mat will bulge up in front of the skidding tires in the form of a moving ripple similar to a "bow wave" (see Figure 7). A major concern is that the "bulging" may exert uplifting forces on the front anchors.

A finite element model was developed to estimate the upper bound of the uplifting forces. NIKE3D, a three-dimensional structural analysis program developed by the Lawrence Livermore National Laboratory (Maker et al. 1991), was used for this study. Taking advantage of symmetry of the problem, only three fiberglass mat panels on half of the repaired crater were included in the model. The rear wheels of the load cart were located 112 cm (44 in) from the rear anchors in the finite element simulation. The asphalt layer
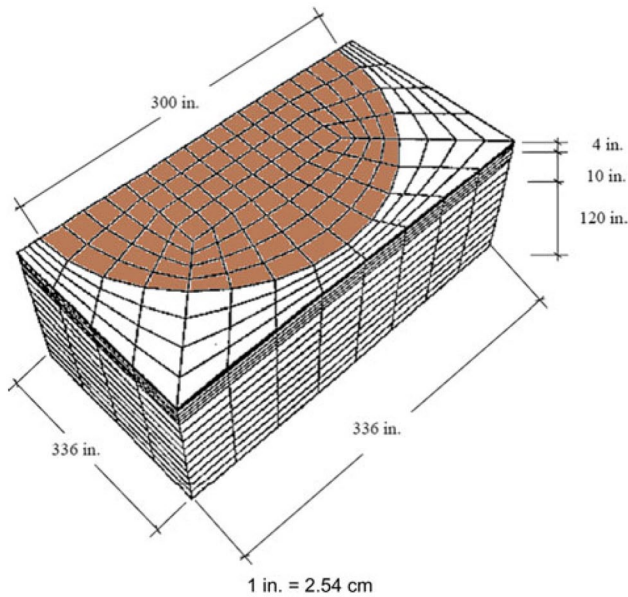
Figure 8. Finite element mesh of the deformable pavement.

Figure 9. NIKE3D simulation of bow wave uplifting force on anchors.

and oyster shell base were modelled with eight-node solid elements, while the fiberglass mat and elastic hinges were modelled with four-node thin shell elements. A frictional sliding interface (coefficient of friction = 0.641) was used to model the contact surface between the fiberglass mat (shell elements) and the repaired crater (solid elements). All material properties were assumed to be elastic and isotropic, and the previously determined values were used in the model. The finite element mesh of the 102-mm (4-in) asphalt layer and the 254-mm (10-in) thick oyster shell base course on top of 3m (10 ft) of beach sand is shown in Figure 8, where the 7.6-m (300-in) diameter, 46-cm (18-in) deep repaired crater is marked by dark color. By changing the material properties of the elements within the crater, the effect of having an underlying crater on the anchor loads could be readily determined. The finite element mesh of the fiberglass mat is shown in Figure 9, where elliptically shaped tire footprints, each with a major axis of 54.6 cm (21.5 in) and a minor axis of 41.9 cm (16.5 in), are built in the mesh. The wheel loads were applied as a uniform contact pressure of 1 MPa (145 psi) on each of the three tire footprints. There were 57 nodes in a tire footprint mesh, and a horizontal force of 147 × 0.662/57 = 1.71 kN (383 lbs) was applied to each node due to skidding. This horizontal force causes the mat to slide towards the front anchors. The initial geometry of the mat was given a slight cylindrical arc in front of the wheels to initiate the bow wave formation. The nodes along the front edge of the mat were fixed to simulate anchors while the back edge of the mat was free to move. In the load cart test, as the tires moved towards the front anchors, the bulge in the mat would slip under the tires and gradually diminish due to constraints by the front anchors. Because the tire footprints were built in the mat mesh, there was no slippage between the tires and the mat. The simulation was
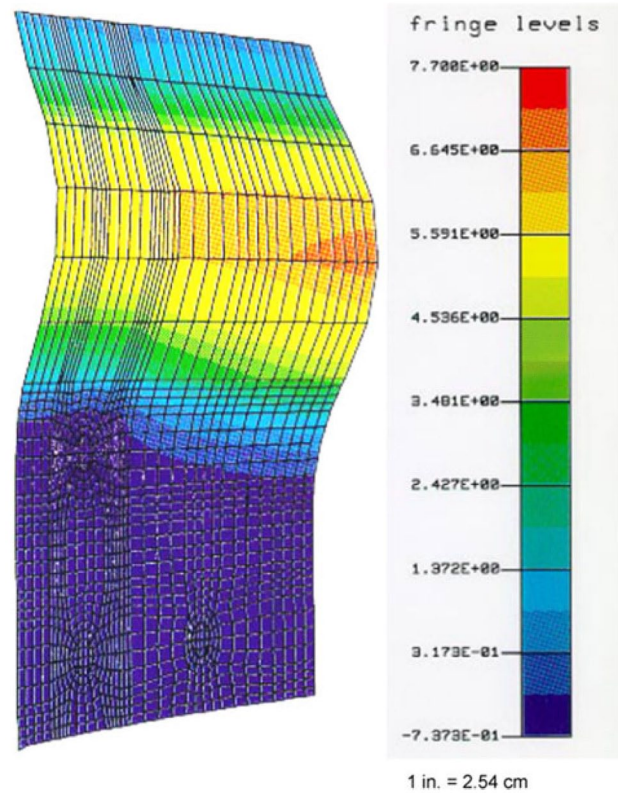
stopped when the bulge was about 195mm (7.65 in) which was close to that observed in a C-5 load cart test shown in Figure 7. The maximum uplifting force on the front anchors was estimated to be about 1.34 kN (300 lbs). The shape of the bulge predicted by NIKE3D (see Figure 9) bears remarkable similarities to that shown in Figure 7. The bulge would form when the compressive stresses in the mat in front of the tires were high to cause the mat to buckle.

Load–deflection characteristics of the current anchoring system

Prior to conducting the load cart tests, a series of destructive tests was conducted on a single mat panel anchored by a single polymer plug anchor in the asphalt pavement to develop a load–deflection curve. Typical levels of anchor load and mat displacement for their corresponding modes of failure are depicted in Figure 10. These tests were conducted at the test site in Florida during summer with temperature well above 32°C (90°F). The modes of failure observed were bearing failure of asphalt around polymer plug, fraying of mat fibers around bushing followed by rock bolt tearing the mat and pull-out of polymer plug after bearing failure in the asphalt was initiated. Bearing failure in the asphalt was most common when pavement temperature was above 38°C (100°F).
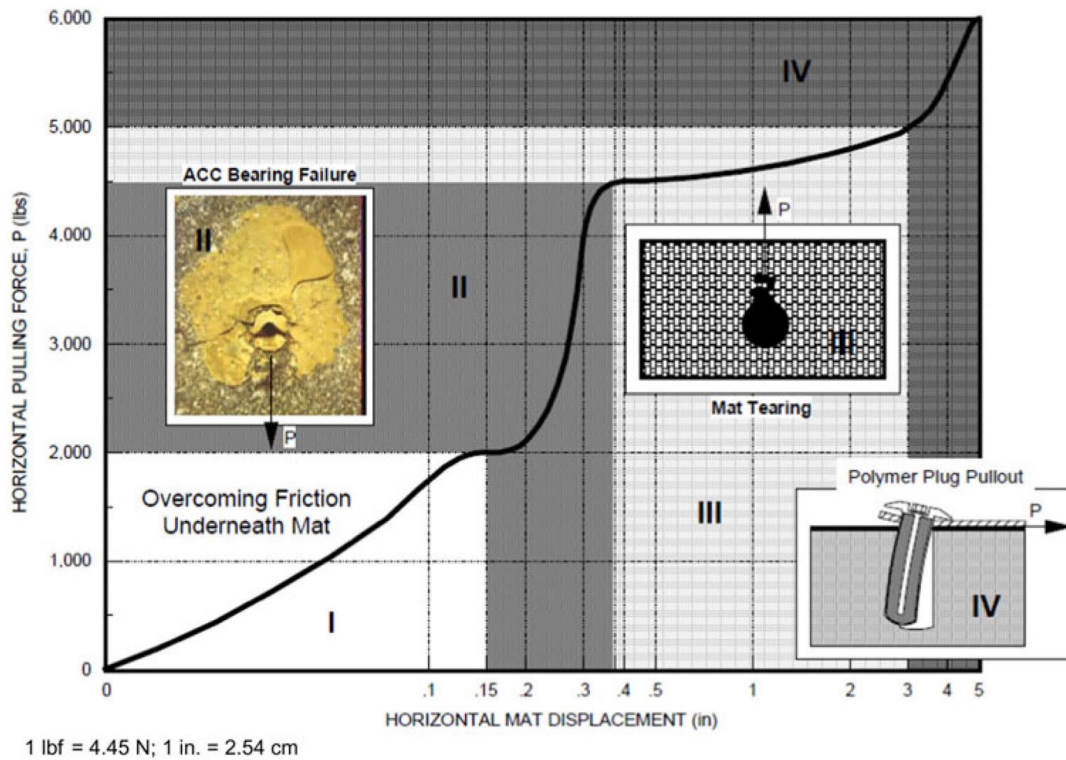
Figure 10. Experience-based load–deflection curve of polymer anchor in asphalt pavement.

A series of vertical pull-out tests was conducted to determine the failure modes and pull-out capacity of the polymer plugs in asphalt pavement for different ambient temperatures. The results are summarized in Table 4. The average pull-out capacity of the polymer plugs was about 15.6 kN (3500 lbs). It proved to be advantageous to install a washer on the bolt end to ensure full embedment in the polymer plug to achieve maximum pull-out capacity.

C-5 load cart field experiments

Tests to measure the anchor loads resulting from full braking (at the skid condition) were performed by statically pulling

a C-5 load cart on an FFM. The load cart was equipped with six C-5 tires that had the same configuration of a single C-5 main gear. The brakes of the load cart were locked up using 27.6 MPa (4000 psi) hydraulic pressure. The tow points of the load cart were about 20 cm (8 in) above the mat. The load cart weighed 16,780 kg (37,000 lbs) and was ballasted to 89,800 kg (198,000 lbs) with 92 lead blocks, weighing approximately 794 kg (1750 lbs) each. The lead blocks were stacked in the cart load box in such a way that each tire carried approximately the same static weight (i.e. 147 kN (33,000 lbs)) when the load cart was pulled across the mat. With an inflation pressure of 1 MPa (145 psi), the tire footprints were elliptically shaped with a major axis of 54.6 cm

Table 4. Summary of vertical anchor pull-out tests (rock bolts in polymer plugs in asphalt pavement).

Test no.	Temperature °C (°F)	Description	Failure mode	Pullout force kN (lbs)
1	29 (85)	Flares not deployed	Bolt pulled out of polymer plug	11.8 (2650)
2	29 (85)	Flares fully deployed	Bolt pulled out of polymer plug	11.1 (2490)
3	29 (85)	Flares manually bent outward	Polymer plug pulled out of asphalt	14.4 (3230)
4	24 (75)	Flares fully deployed	Polymer plug pulled out of asphalt	17.7 (3970)
5	24 (75)	Flares fully deployed	Polymer plug pulled out of asphalt	15.7 (3520)
6	24 (75)	Washer installed on bolt end	Polymer plug pulled out of asphalt	13.5 (3040)
7	24 (75)	Washer installed on bolt end	Polymer plug pulled out of asphalt	20.2 (4540)
8	24 (75)	Flares fully deployed	Polymer plug pulled out of asphalt	18.0 (4040)
9	24 (75)	Flares fully deployed	Polymer plug pulled out of asphalt	16.5 (3710)
10	24 (75)	Washer installed on bolt end	Polymer plug pulled out of asphalt	19.2 (4310)
11	24 (75)	Washer installed on bolt end	Polymer plug pulled out of asphalt	14.7 (3310)

(a)

Load Cart Towing Configuration

(b)

Front View

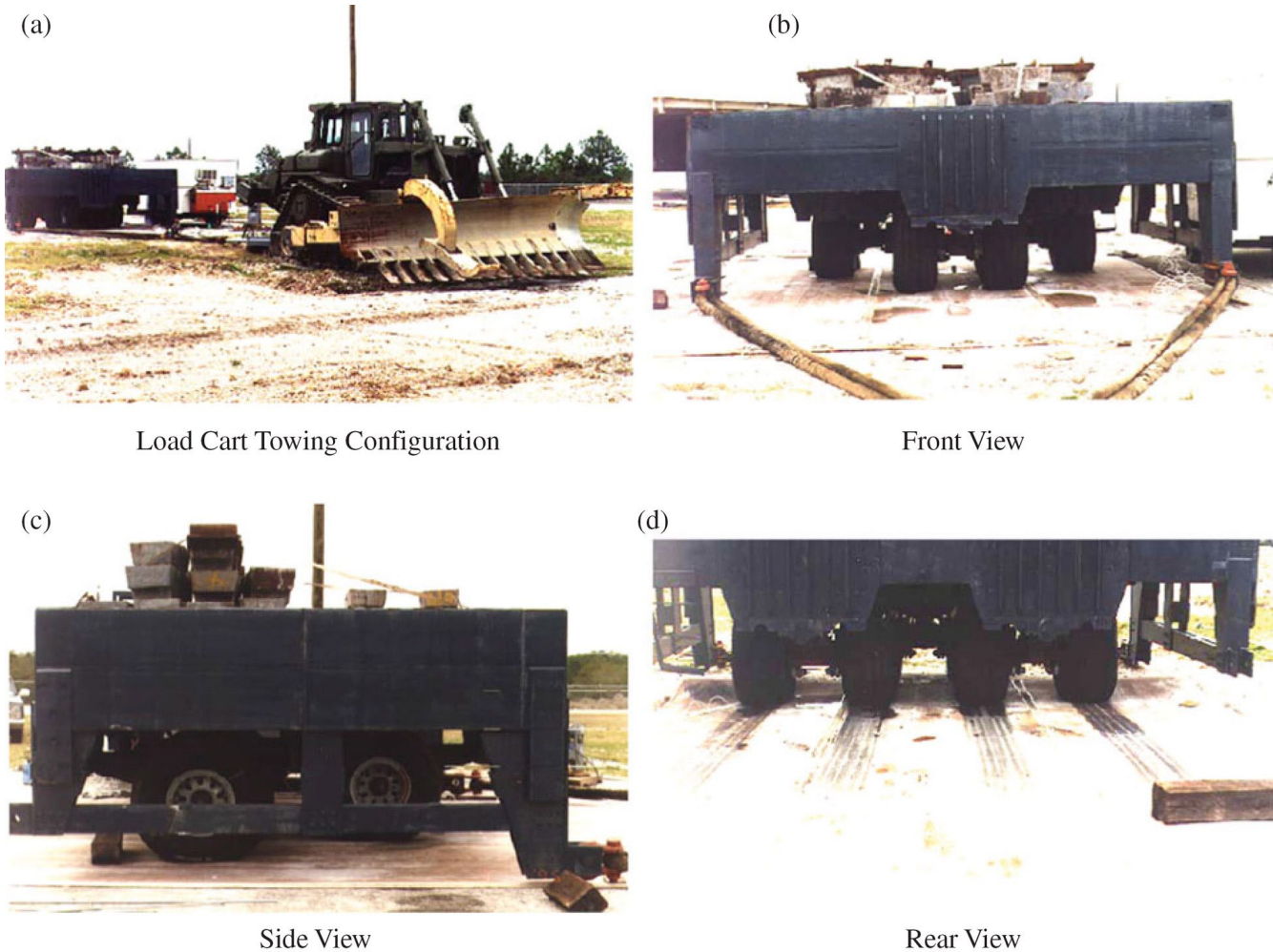(c)

Side View

(d)

Rear View

Figure 11. C-5 load cart.

(21.5 in) and a minor axis of 41.9 cm (16.5 in) under the 147-kN (33,000-lb) wheel load. The C-5 load cart towing configuration, front view, side view and rear view are shown in Figure 11(a)–(d), respectively.

Anchor load measurement

It was necessary to develop a device for measurement of the horizontal loads transferred from the fiberglass mat to the anchors, while maintaining all of the essential performance characteristics of the existing system, i.e. the mat, the anchor and the pavement. This force measurement system was developed by strain gauging an anchor bushing. The bushings are made of steel, which has linear elastic deformation behavior under operational loads in the load tests.

Bushing load cell development

Figure 12 shows loads acting on an anchor bushing. A horizontal load applied to the mat, such as that due to braking, is transferred as a horizontal compressive load on the anchor bushing, which, in turn, exerts a horizontal compressive

load on the anchor bolt. The anchor bolt in the current system is a 12.7-mm (0.5-in) diameter, 241-mm (9.5-in) long rock bolt, typically used for concrete pavements with up to 152mm (6 in) of asphalt overlay. The load on the bolt is reacted by the pavement acting on the embedded portion of the bolt. The force pair represented by the arrows is the only one measured by the anchor bushing load cell. If the bolt is torqued down, the compressive stress induced between the mat and the pavement would allow load transfer by friction. However, the anchor bushing load cell is intended for use with anchors in asphalt pavement, where the anchor bolt will be embedded in a polymer plug poured in a 38-mm (1.5-in) diameter hole in the pavement. In this case, the bolts are not to be torqued down. Thus, there will be no normal (compressive) force acting between the mat and the pavement, and the anchor loads will be carried in horizontal shear by the bolt and not by friction.

As shown in Figure 13, four strain gauges were installed on each bushing in a full bridge configuration. Only two of the gauges actually sense load at any one time, either the two on the right or the two on the left. The full bridge was
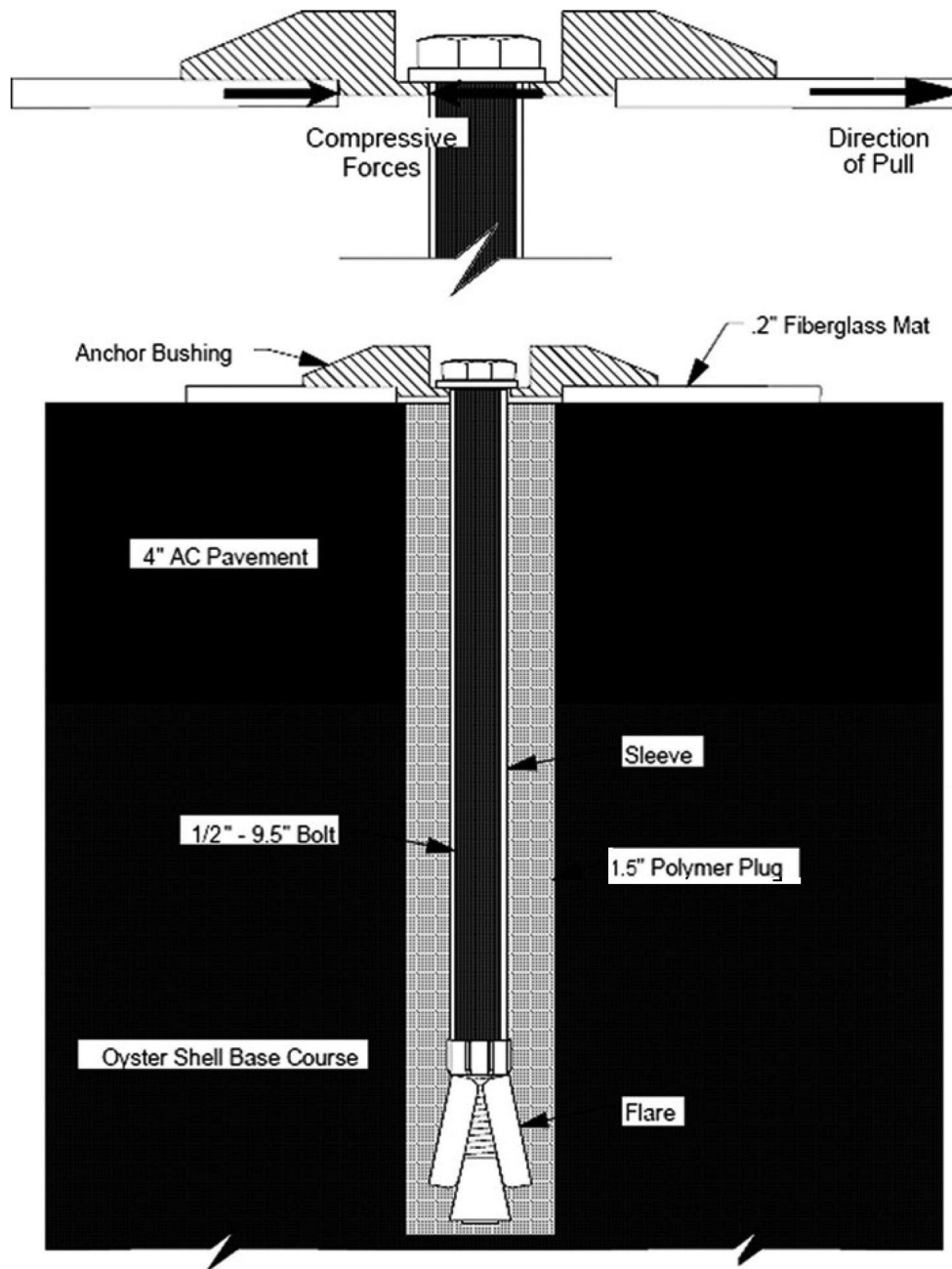
Figure 12. Bushing load cell concept.

included for temperature compensation and for compensation for bending stresses in the bushing flange. Because of the inclusion of two gauge stations, the bushing load cell can be calibrated to measure load in either the positive or the negative direction along the gauged axis, a useful feature if trafficking were being performed in both directions. Because the strain-gauged section of the bushing is close to the contact points, the load cell output is influenced by the characteristics of the contact between the bushing and the bolt. The bushing load cells have a measurement uncertainty of approximately 890–1780N (200–400 lbs).

Bushing load cell validation

A 1.2-m (4-ft) long, 46-cm (18-in) wide piece of fiberglass mat was used for a pull test to validate the bushing load cell, as shown in Figure 14. The anchor was installed in a concrete pavement to provide a targeted peak anchor load of 26.7 kN (6000 lbs) for validation. A load cell was placed in line to measure the pulling force. A hardened sleeve was placed in the bushing with its top flush with the top of the anchor bolt opening. A rock bolt was snugly fitted into the sleeve such that the washer was only in contact with the
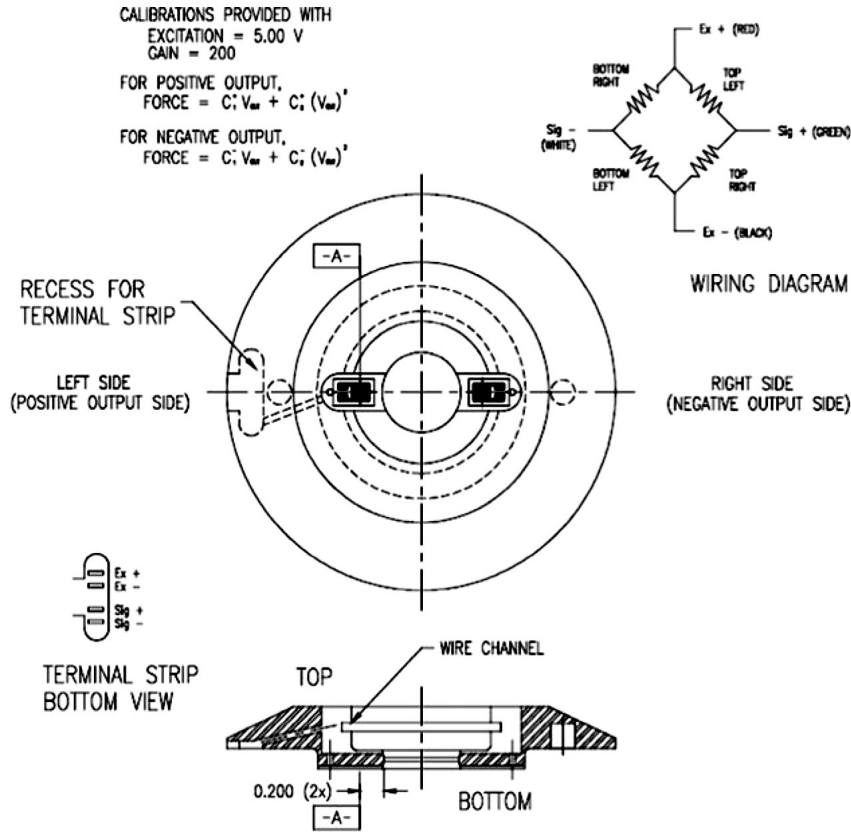
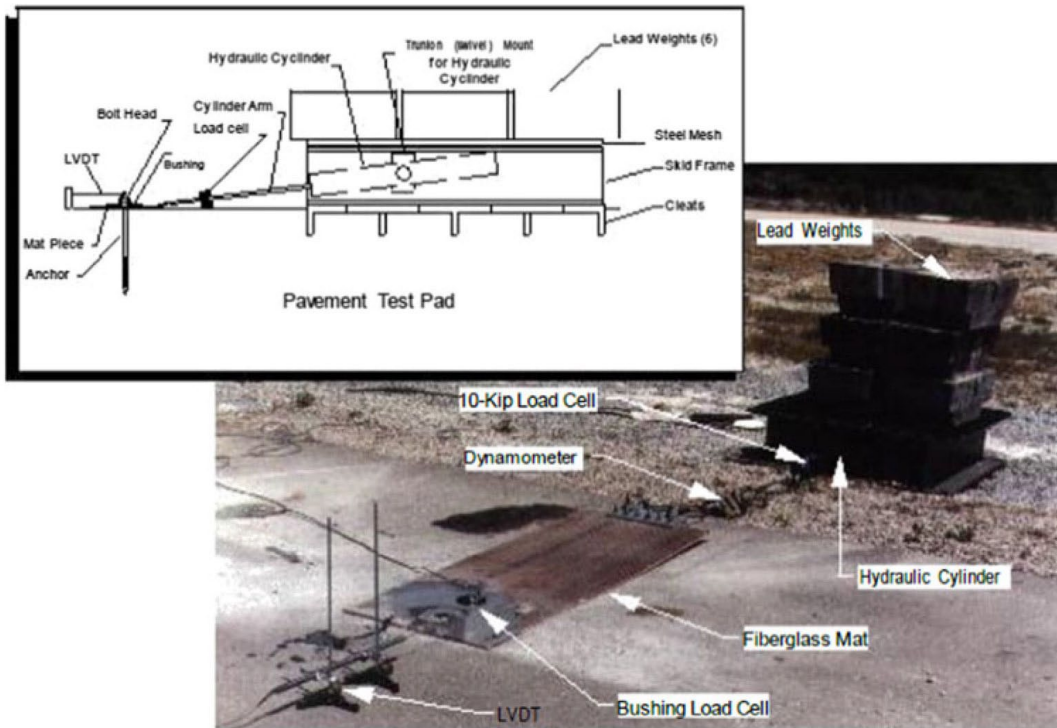**Figure 13.** Bushing load cell strain gauge detail.

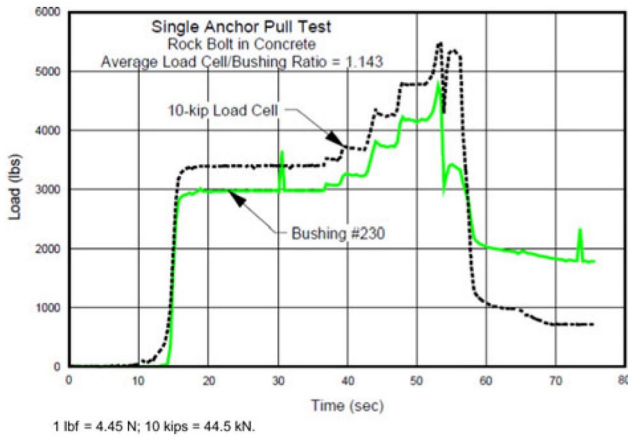**Figure 14.** Single anchor pull test for bushing load cell validation.

Figure 15. Field validation of bushing load cell.

sleeve and the bushing was still free to rotate after the bolt was torqued down. The bottom surface of the mat around the bushing hole was lubricated and a wood wedge was placed under the mat behind the bushing to prevent the mat from lodging underneath the bushing. A hydraulic cylinder was used to gradually apply a pulling force to the mat and the anchor. The bushing load cell and reference load cell data are compared in Figure 15. The bushing load cell traced the applied load very closely during loading. However, significant deviation from the reference load trace was noted during unloading. The bushing load cells relied on the pair of compressive forces shown in Figure 12 to sense anchor loads. In general, the bushing load cell underestimated the actual anchor load by about 14%. However,

these load cells became ineffective once the mat slipped underneath the bushing. As a result, there is no physical significance to the unloading portion of the load trace shown in Figure 15. A correction factor of 1.14 was applied to all load cell data.

C-5 load cart tests

A fiberglass mat was laid out and anchored with 38-cm (1.5-in) diameter polymer plugs. Six load cart skid tests were conducted at two locations on the mat. These tests were conducted when the asphalt pavement temperature was about 16°C (60°F). The pulling forces on the load cart were applied at one-third, two-thirds and full extent of the 579-kN (130,000-lb) braking force. Reduced pulling forces were used to simulate the anchor loads produced by an anti-skid brake system. In addition to 28 instrumented bushings and the load cell, a string potentiometer was tacked on the mat under the rear axles of the load cart to detect mat slippage. Because the static coefficient of friction between the mat and the asphalt pavement was determined to be 0.564, no mat slippage was expected until the pulling force reached about 881 × 0.564 ≅ 497 kN (112,000 lbs) when sudden increases in anchor forces occurred as soon as the mat slipped. The front anchors were not subject to significant horizontal loads due to bow wave formation. The bushing load cells along the leading edge of the mat were unable to sense the uplifting forces due to mat buckling. The peak horizontal loads measured by the load cells along the back edge of the mat are compared with the values predicted by the simplified model in Figures 16 and 17.
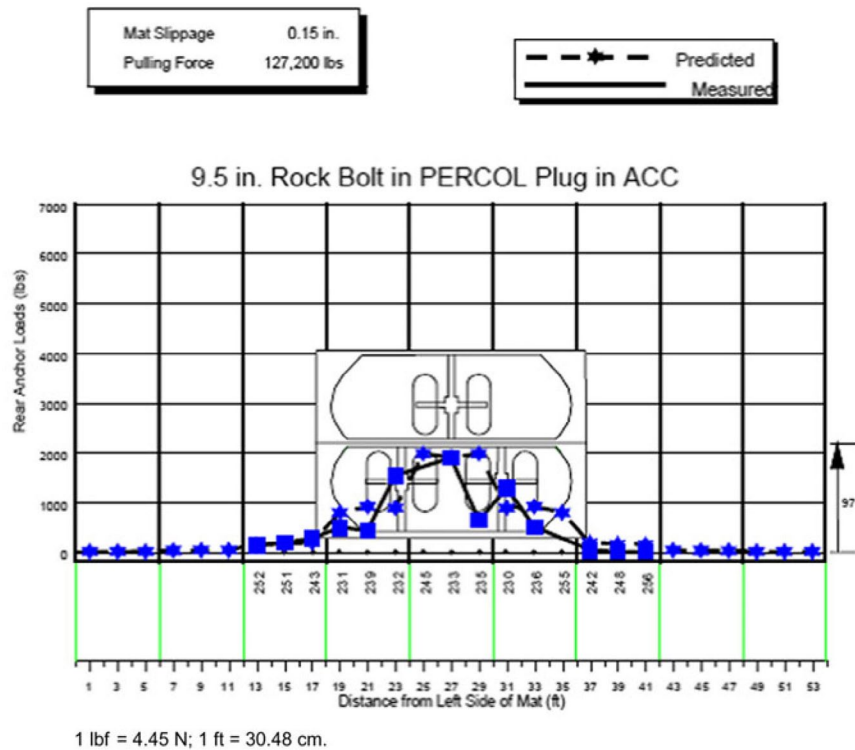

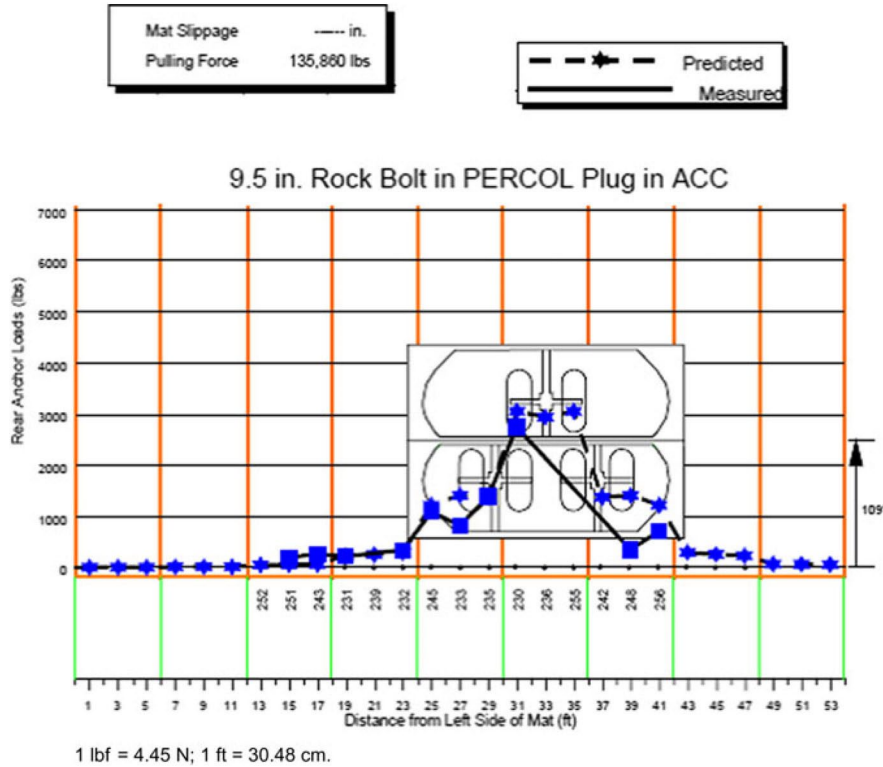**Figure 16.** Peak anchor load distribution in load cart test #3.

Figure 17. Peak anchor load distribution in load cart test #6.

Load cart tests on repaired crater with polymer plugs in asphalt

A fiberglass mat was placed over the repaired crater and anchored with polymer plugs in the asphalt pavement. The 89,800-kg (198,000-lbs) C-5 load cart was placed on the mat over the repaired crater as shown in Figure 18. The wheels of the load cart were locked up and the rear axles were measured at 4m (157 in) from the rear anchors. Only the rear anchors of the middle three fiberglass panels were instrumented to measure horizontal anchor loads. The displacement of the middle anchor in each of the three panels was monitored with an LVDT. These tests were conducted when the asphalt pavement temperature was about 16°C (60°F).
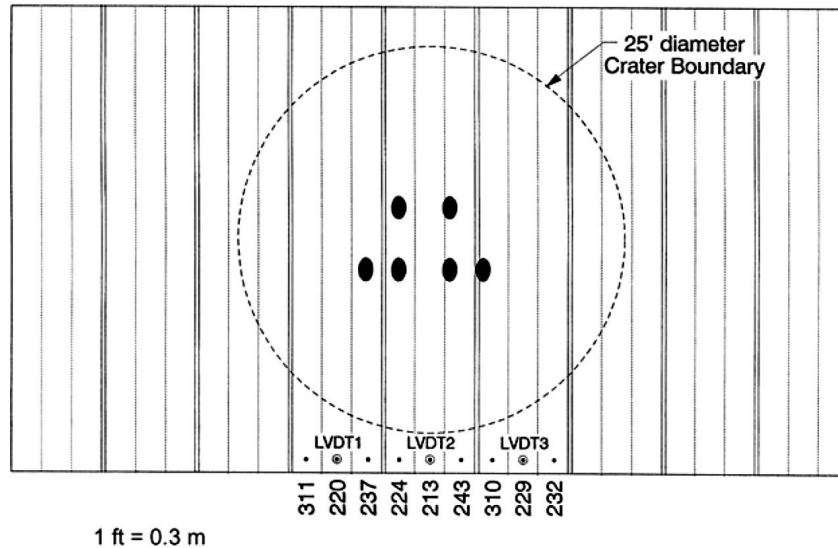

Figure 18. Location of bushing load cells and LVDTs for load cart tests on a repaired crater.
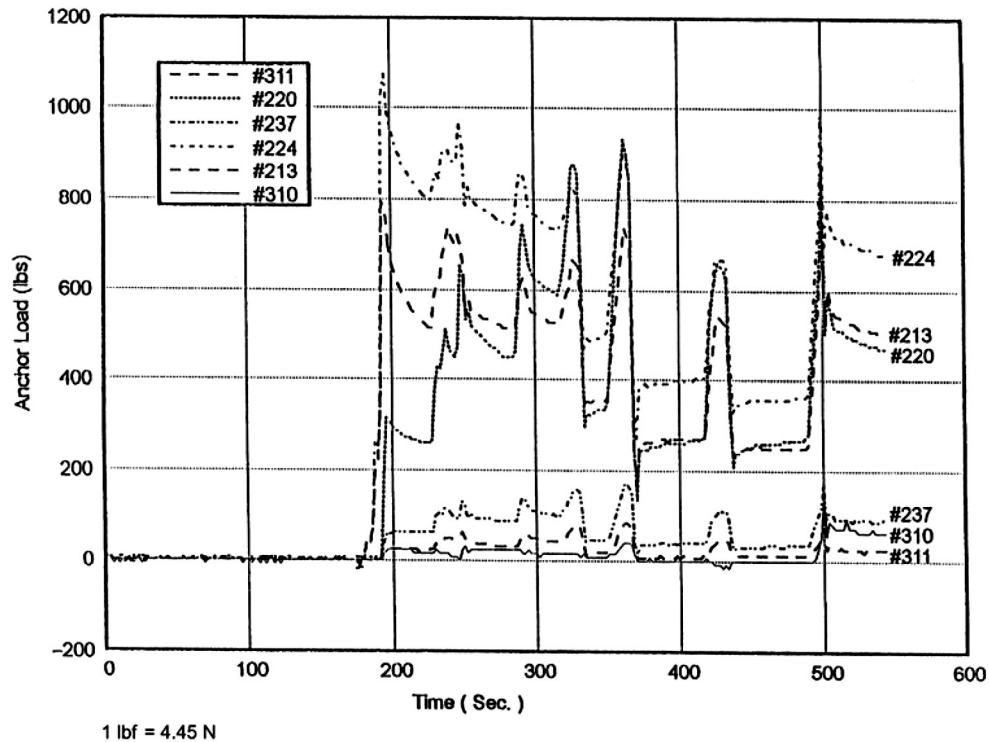
Figure 19. Anchor loads due to C-5 load cart rolling onto the mat.

Anchor loads due to initial settlement of repaired crater

The transient anchor loads resulting from rolling the load cart onto the mat over the repaired crater are shown in Figure 19. The average load data indicate that anchor loads would be around 2.2 kN (500 pounds), after the load cart was rolled on the mat. This value occurred during the initial settlement in the repaired crater under wheel loads at about 550 s. These horizontal anchor loads are caused by the instantaneous settlement under the heavy wheel loads. Although an instantaneous peak horizontal load of about 4.9 kN (1100 lbs) was measured, the average load on the anchors under the initial settlement would be around 2.2 kN (500 lbs).

Anchor loads due to 500 cycles of repeated loading

For expedient repair, UFC 3-270-07 (2003) specifies that the repair should sustain 100 C-17 passes with a gross weight of 227,707 kg (502 kip), or 100 C-130 passes with a gross weight of 79,380 kg (175 kip), or 100 passes of a particular aircraft at its projected mission weight if other than the C-17 or C-130, or the number of passes required to support the initial surge mission aircraft. The polymer plug anchors subjected to 500 cycles of repeated loading were intended to cause cumulative damage (or fatigue failure) under horizontal braking forces.

The stroke of the hydraulic cylinder was extended and retracted in a cyclic fashion to apply the repeated loading. For the first 125 cycles, the range of the applied load cycles was between 44.5 and 200 kN (10,000 and 45,000 lbs). Each cycle took about 50 s. Because the first 125 cycles were applied right after the load cart had been rolled on the mat, the anchor loads and displacements were caused by the combined effect of settlement of the repaired crater and the cyclic loading. Bushings #213 and #220 displaced about 0.76mm (0.03 in), while bushing #229 displaced about 1mm (0.04 in). The maximum static anchor load measured was 2.8 kN (620 lbs).

The next 250 cycles of repeated loading were conducted the day after the first 125 cycles, and the settlement of the crater repair material should have been stabilized by that time. The range of the applied load cycles was between 2.2 and 200 kN (500 and 45,000 lbs). On the average, bushings #220 and #229 displaced 0.38mm (0.015 in) and bushing #213 displaced 0.71mm (0.028 in). The maximum anchor load induced by the cyclic loading was 890N (200 lbs). Another 125 cycles of repeated loading between 2.2 and 200 kN (500 and 45,000 lbs) were conducted the next day. As before, bushings #220 and #229 displaced 0.38mm (0.015 in) and bushing #213 displaced 0.76mm (0.03 in). The maximum anchor load induced by the cyclic loading was 779 kN (175 lbs). The change of loading and the number of cycles were predetermined to apply in three stages to inspect cumulative damage in the polymer plug anchors.
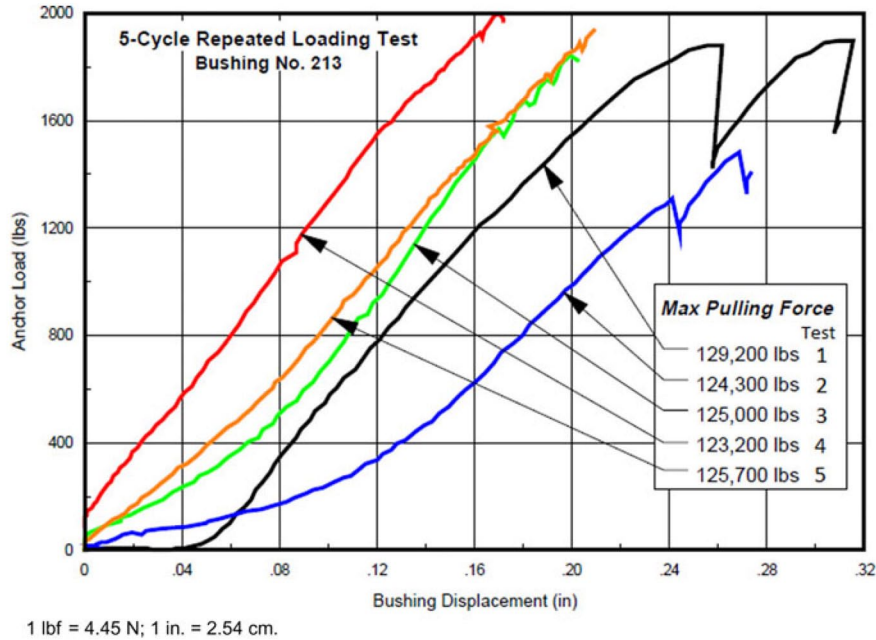
Figure 20. The load–deflection curves obtained in the low-cycle fatigue loading tests.

Anchor loads due to five cycles of C-5 load cart skidding forces

The polymer plug anchors sustained the 500 cycles of repeated loading between 2.2 and 200 kN (500 and 45,000 lbs) with no visible damage. This anchoring system was subsequently subjected to five cycles of the full braking forces of the C-5 load cart. In this series of tests, the load cart brakes were released, the load cart was rolled off the fiberglass mat and the data acquisition was reset after each loading. The same loading and unloading sequence was repeated five times to evaluate the low-cycle fatigue behavior of the polymer plug anchors. The load– displacement curves for bushing #213 of the five tests are given in Figure 20. The slopes of these curves represent the stiffness of polymer plug anchors in thin asphalt pavement. Any reduction in the slope in the subsequent tests would indicate degradation of the

anchor stiffness. The maximum pulling forces, anchor loads and displacements, and the anchor stiffness obtained in the five-cycle load cart test are summarized in Table 5. Based on the test data presented in Table 5, it can be shown that anchor load = anchor (or mat) displacement × anchor stiffness. The anchor stiffness values calculated from the test data compare favorably with the 2.1 kN/mm (12,000 lbs/in) value reported by Adcock et al. (1993). A post-test inspection of the anchors revealed that the mat lodged underneath several bushings, causing premature data termination in #237, #310 and #232. No visible damage was noticed in the mat or the polymer plug anchors.

Anchor load predictions using simplified model

The simplified model developed for anchor load predictions has proven to be very accurate when validated against load

Table 5. Summary of data from the five-cycle low-cycle fatigue tests.

Test number	Peak pulling forces kN (kip)	Maximum anchor loads kN (lbs)	Maximum mat displacements mm (in)	Anchor stiffness kN/mm (lbs/in)
1	575 (129.2)	10.4 (2330)	5.46 (0.215)	1.90 (10,832)
2	553 (124.3)	6.6 (1493)	4.57 (0.180)	1.44 (8295)
3	556 (125.0)	8.7 (1965)	4.34 (0.171)	2.00 (11,479)
4	548 (123.2)	8.9 (1999)	3.78 (0.149)	2.35 (13,428)
5	559 (125.7)	8.6 (1935)	4.88 (0.192)	1.76 (10,075)
Average	558 (125.5)	8.7 (1944)	4.60 (0.181)	1.89 (10,822)

cart test data. An effective tension stiffness of 2.1 kN/mm (12,000 lbs/in) for mats anchored with polymer plugs in asphalt was derived from the load cart test data and used in the model. This model was then used to predict the maximum anchor loads caused by the full braking force from various aircraft. The predicted maximum anchor loads for these aircraft are summarized in Table 6.

Conclusions

A research effort consisting of analytical studies, materials testing and field experiments has been carried out to evaluate the adequacy of using polymer plugs to anchor FFMs on repaired crater in thin asphalt pavements under simulated braking forces of heavy cargo aircraft. An 89,800-kg (198,000-lb) load cart having the footprint of a single C-5 main gear was pulled on an FFM with all the wheels locked to simulate the full braking force, and the resulting anchor loads were measured. Load cart tests were conducted on a mat anchored with polymer plugs in asphalt as well as on a mat over a 7.6-m (25-ft) diameter, 46-cm (18-in) deep crater repaired using a well-graded aggregate mix per ASTM D2940. The current mat anchoring system survived the full braking forces in all the load cart tests with no visible damage; however, it should be noted that the load cart tests were conducted at relatively low asphalt pavement temperature of about 16°C (60°F). Bearing failure in the asphalt pavement is likely to occur at an anchor load of more than 8.9 kN (2000 lbs) when the pavement temperature is above 38°C (100°F).

Repetitive loading effect

A repeated loading of 500 cycles between 2.2 and 200 kN (500 and 45,000 lbs) was conducted using the C-5 load cart to estimate the allowable passes on an FFM over a repaired crater. Another five cycles of load cart tests were subsequently conducted to evaluate the low-cycle fatigue performance of the anchoring system under the full braking forces. The polymer plug anchors and the mat survived the repeated loading with no visible damage. Heavy aircraft trafficking would also cause compaction and rutting of the underlying repaired crater. Sagging of the FFM due to the settlement would cause an increase in anchor loads of about 2.2 kN (500 lbs).

Polymer plug anchor capacities

A depression basin will form under the heavy wheel loads of a cargo aircraft on a mat with an underlying repaired crater. A bulge or "bow wave" of significant magnitude may form in front of the aircraft wheels during braking. The maximum uplift force caused by bow wave was estimated to be about 1.3 kN (300 lbs). The average vertical pull-out capacity of the polymer plugs was 15.6 kN (3500 lbs), which is much higher than the maximum uplifting force estimated from finite element simulation.

Table 6. Predicted maximum anchor loads due to aircraft full braking.

Aircraft	Maximum take-off weight kN (pounds)	Maximum single wheel load kN (pounds)	Maximum predicted anchor load kN (pounds)
F-15 C/D	303 (68,000)	132 (29,600)	3.24 (728)
KC-135R	1,435 (322,500)	168 (37,700)	11.95 (2685)
C-141B	1,438 (323,100)	169 (38,100)	11.12 (2498)
C-130 H	779 (175,000)	186 (41,900)	7.52 (1690)
C-17A	2,581 (580,000)	198 (44,500)	14.06 (3160)
C-5B	738 (840,000)	146 (32,800)	21.05 (4730)

The anchor loads and stiffness are associated with horizontal braking force. The horizontal loads on the anchors due to the worst-case braking scenario have been measured in C-5 load cart tests. The polymer plug anchors have adequate load capacity and anchor stiffness that passed both high-cycle and low-cycle fatigue loading tests.

Anchor load predictions using simplified model

The simplified model developed for anchor load predictions has proven to be very accurate when validated against load cart test data. This model is useful for predicting the maximum anchor loads caused by the full braking force from various aircraft. Based on the data in Table 6, the max anchor loads from all the heavy cargo aircraft (except C-130) are higher than the C-5 load cart test anchor loads in Table 5. Taking into account that C-5 and other heavy cargo aircraft are equipped with anti-skid brakes, and that having multiple main gears braking on the same mat panel is not likely, the polymer plug anchors might be adequate for use in asphalt runway pavements. Further investigation is warranted.

References

Adcock, A.D., Dass, W.C., Lee, X., and Timian, D.A., 1993. Methods for anchoring the USAF folded fiberglass mat to flexible and unpaved aircraft operating surfaces. Air Force Materiel Command, Wright Laboratory, Air Base Technology Branch, Tyndall Air Force Base, FL, Final Report WL-TR-93-3517, June.

Barker, W.R. and Gonzalez, C.R., 1991. Pavement design by elastic layer theory. Proceedings of conference on aircraft/pavement interaction – an integrated system, Kansas City, MO, 4–6 September.

Engineering Technical Letter 07-2, 2007. Anchoring a fiberglass mat assembly in asphalt concrete (AC) pavement, U.S. Air Force Civil Engineer Support Agency, Tyndall Air Force Base, FL, Dec 19, 10 p.

Engineering Technical Letter 07-10, 2007. Evaluation and restoration of folded fiberglass mat (FFM), U.S. Air Force Civil Engineer Support Agency, Tyndall Air Force Base, FL, Dec 19, 21 p.

Holliway, R. and Millard, K.S., 1990. Aircraft characteristics for airfield pavement design and evaluation. Air Force Engineering and Services Center, Tyndall AFB, FL, Aug.

Law Engineering, Inc., 1988. Polyurethane/polyester folded fiberglass mat test properties. Atlanta, GA: Law Engineering, Inc., Test Report Number AM10316.01.

Lester, W.G.S. and Phil, D., 1973. Some factors influencing the performance of aircraft anti-skid systems. Technical Memorandum EP 550, Royal Aircraft Establishment, UK, July, 18 p.

Maker, B.N., Ferencz, R.M., and Hallquist, J.O., 1991. NIKE3D, a nonlinear, implicit, three-dimensional finite element code for solid and structural mechanics. User's Manual, UCRLMA-105268, Lawrence Livermore National Laboratory, Livermore, CA, Jan.

Marzbanrad, J. and Pahlavani, M., 2011. A system identification algorithm for vehicle lumped parameter model in crash analysis. International Journal of Modeling and Optimization, 1 (2), 163–168.

MIL-DTL-32265, 2007. Detail specification sheet, folded fiberglass mat fabrication and packaging, US Air Force Civil Engineer Support Agency, Tyndall Air Force Base, FL, Nov 2, 22 p.

UFC 3-270-07, 2003. Unified facilities criteria: airfield damage repair, June 30, 108 p.